



Optimal multiparameter analysis of source water distributions in the Southern Drake Passage



Marina Frants^{a,*}, Sarah T. Gille^a, Christopher D. Hewes^a, Osmund Holm-Hansen^a, Mati Kahru^a, Aaron Lombrozo^a, Christopher I. Measures^b, B. Greg Mitchell^a, Haili Wang^d, Meng Zhou^c

^a Scripps Institution of Oceanography, University of California, San Diego, La Jolla, CA 92093-0202, United States

^b University of Hawaii, Honolulu, HI 96822, United States

^c University of Massachusetts Boston, MA 02125, United States

^d Xiamen University, Fujian Province, China

ARTICLE INFO

Available online 16 June 2012

Keywords:

Southern Ocean
Drake Passage
Iron
OMP analysis
Ona Basin

ABSTRACT

In order to evaluate the effects of horizontal advection on iron supply in the vicinity of the Shackleton Transverse Ridge (STR) in the southern Drake Passage, the water composition in the region is estimated along the isopycnal containing the subsurface iron peak. Optimal Multiparameter (OMP) analysis of temperature, salinity, oxygen and nutrient data is used to estimate the water composition at CTD stations sampled in summer 2004 and winter 2006. The highest iron concentrations in the Ona Basin are found below the mixed layer, both in summer and in winter. The water composition derived from the OMP analysis is consistent with a scenario in which iron-rich shelf waters from the South Shetland Islands and the Antarctic Peninsula are advected northward on the eastern side of the STR, where they interact with the low-iron waters of the Antarctic Circumpolar Current (ACC) in the Ona Basin. The shelf waters and the ACC waters appear to interact through a stirring process without fully mixing, resulting in a filamented distribution that has also been inferred from the satellite data. To the west of the STR, the shelf waters are primarily confined to the continental shelf, and do not extend northwards. This source of water distribution is consistent with the idea that iron enters the Ona Basin from the continental shelf through advection along an isopycnal, resulting in an iron concentration peak occurring below the winter mixed layer in the Ona Basin.

© 2012 Elsevier Ltd. All rights reserved.

1. Introduction

Satellite-based and *in situ* measurements of phytoplankton abundance in the Southern Ocean show a heterogeneous distribution, with regions of high phytoplankton biomass occurring primarily in shallow waters near islands and continental margins and in deeper waters located downwind and downstream from land features that interrupt the flow field of the Antarctic Circumpolar Current (ACC) between 45° and 60°S (Blain et al., 2001; Sullivan et al., 1993). Since biological productivity in the pelagic Southern Ocean is primarily iron-limited (Boyd, 2002; Chisholm and Morel, 1991; de Baar et al., 1995; Martin et al., 1990), these observations suggest that phytoplankton biomass in the open ocean is increased by the redistribution of iron from shelf waters into pelagic waters in regions where mixing between waters from different sources is enhanced by topographic

features (Holm-Hansen et al., 1997, 2004). However, the physical processes that drive the regional differences in iron distribution are not yet well understood (de Baar and de Jong, 2001). A number of possible mechanisms have been examined. Whitehouse et al. (2008) found evidence of nutrient upwelling resulting from diverging flow of the ACC over the shelf near South Georgia Island. Sokolov and Rintoul (2007) have found that similar upwelling occurs wherever the ACC interacts with topography. Hewes et al. (2009) observed that shallow mixed-layer depths contribute to increased Chl-a levels near the South Shetland Islands. *In situ* observations near the Kerguelen Plateau (Blain et al., 2001) and the Crozet Plateau (Venables et al., 2007) suggest that sediment mixing in shallow waters near islands and continental shelves, followed by downstream advection, can supply iron to facilitate blooms in off-shore waters.

In this study, we examine the water properties in the vicinity of the Shackleton Transverse Ridge (STR) in Southern Drake Passage near the Antarctic Peninsula (Fig. 1A). The STR runs diagonally across our study region, extending northwest into Drake Passage from Elephant Island (see Fig. 1B). The shallowest depth over the ridge is approximately 800 m, while the basins on

* Corresponding author at: Scripps Institution of Oceanography, University of California, San Diego, La Jolla, CA 92093-0230, United States.

E-mail address: mfrants@ucsd.edu (M. Frants).

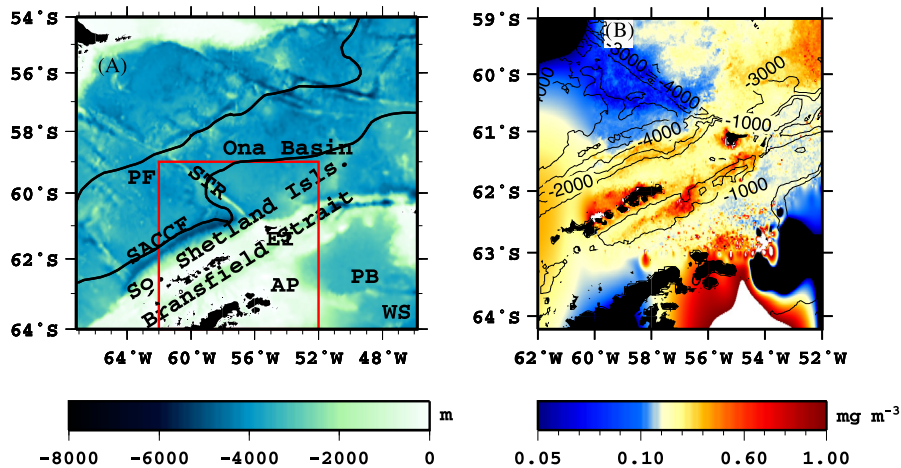


Fig. 1. (A) Drake Passage bathymetry with study region indicated by the red rectangle. Front definitions are taken from Orsi et al. (1995). The abbreviations are: Shackleton Transverse Ridge (STR), Elephant Island (EI), Polar Front (PF), Southern ACC Front (SACCF), Antarctic Peninsula (AP), Powell Basin (PB) and Weddell Sea (WS). (B) A composite of Chl-a distribution in the study region from January 1 to March 31 2004, computed from SeaWiFS and MODIS-Aqua satellite data. (For interpretation of the references to color in this figure caption, the reader is referred to the web version of this article.)

either side reach depths of over 4000 m; the gap between the ridge and Elephant Island has a depth of over 3000 m. The flow of the ACC around the topography creates a region of high mixing, as the meridional meandering of the Southern ACC Front (SACCF) brings the ACC waters into close proximity with the shelf waters off the Antarctic Peninsula and the South Shetland Islands (Orsi et al., 1995), as well as with the Weddell Sea waters flowing north toward the Scotia Sea (Barré et al., 2008; Brandon et al., 2004; von Gyldenfeldt et al., 2002; Whitworth et al., 1994).

Satellite-derived Chlorophyll-a (Chl-a) images in this region (Kahru et al., 2007) show a sharp gradient in surface chlorophyll levels in the vicinity of the STR (Fig. 1B). Low Chl-a water is located to the west of the ridge, and high Chl-a water is found to the east in the Ona Basin and continues downstream into the southern Scotia Sea. Shipboard iron incubations conducted across the gradient have shown that phytoplankton biomass in the western Drake Passage is iron-limited, except in the shallow waters on the continental shelf (Helbling et al., 1991; Hopkinson et al., 2007). The incubation results, together with the low iron levels measured in the ACC west of the STR by Martin et al. (1990), the iron distributions reported by Ardelan et al. (2010), and the Chl-a distributions shown by Kahru et al. (2007), suggest that the Ona Basin consistently has higher levels of iron than the surrounding waters.

Previous studies of hydrographic data in the vicinity of the STR and the Antarctic Peninsula show the presence of Circumpolar Deep Water (CDW), Bransfield Strait Water (BW) and Weddell Sea Deep Water (WSDW) (Hofmann et al., 1996; Whitworth et al., 1994; Zhou et al., 2010b). The water column of the ACC is characterized primarily by CDW, overlaid by Antarctic Surface Water (ASW) during the summer. On the continental shelf, interaction between these water masses, combined with the effects of local cooling, ice melt and precipitation effects, form the shelf waters (Hofmann et al., 1996; Zhou et al., 2002, 2010b). Shelf waters flowing northward from the Weddell Sea branch at the northern tip of the peninsula, with some of the waters flowing eastward into the Weddell-Scotia Confluence and some flowing westward and contributing to the formation of the BW (Hofmann et al., 1996; Zhou et al., 2002). The BW, in turn, combines with the CDW from the ACC to form the shelf waters around the South Shetland Islands (Hofmann et al., 1996; Zhou et al., 2002). Since the shelf waters are iron-rich compared to the ACC waters (Hopkinson et al., 2007), their distribution affects biological productivity throughout the region.

To understand the iron sources associated with the water masses in our study region and the horizontal transport and mixing mechanisms, we will use Optimal Multiparameter Analysis (OMP) (Tomczak and Large, 1989) to estimate the relative contributions of these waters for a region comprising the deep basins to the east and west of the STR, the gap to the south of the STR, and the continental shelf along the South Shetland Islands. Our analysis is based on the assumption that advection moves water primarily along isopycnals; therefore we examine source water distributions for the isopycnal layer where the iron concentrations are highest in both summer and winter. We also perform the analysis for the density range below the iron peak, where water properties are more uniform and source water definitions are more distinct. Use of the OMP method allows us to assess quantitatively the horizontal propagation of iron-rich shelf waters within our study region.

2. Data and methods

Two cruises were conducted in the vicinity of the STR to study oceanographic transport and its possible influence on biological activity in the Ona Basin. In February and March 2004, the A.S.R.V. *Laurence M. Gould* (LMG0402) collected hydrographic, chemical and biological data in the vicinity of the STR. In July and August 2006, the I.B.R.V. *Nathaniel B. Palmer* (NBP0606) revisited the area to collect similar measurements. In addition, a survey by the U.S. Antarctic Marine Living Resources (AMLR) Program was conducted in January and February of 2004, overlapping with LMG0402. The locations of all the hydrographic stations are shown in Fig. 2.

A total of 121 casts were made during LMG0402 and 192 casts were made during NBP0606, all to 1000 m or 10 m above the bottom, whichever was shallower. Each station included a rosette-CTD cast using a rosette from the Raytheon Polar Service Company (RPSC) and/or a Trace Metal Clean (TMC) rosette-CTD cast using a rosette from the University of Hawaii (Measures et al., 2008). Temperature, salinity and oxygen measurements were sampled during each RPSC and TMC cast using a SBE911 CTD and a SBE42 oxygen sensor. In addition, samples for measuring phosphate, nitrate and silicate concentrations were taken from bottles mounted on each rosette, with 12 bottles per cast.

The 2004 NOAA-AMLR survey performed 91 CTD casts during Leg 1 (January–February) and 98 casts during Leg 2 (February–March), using a Sea-Bird CTD mounted on a rosette

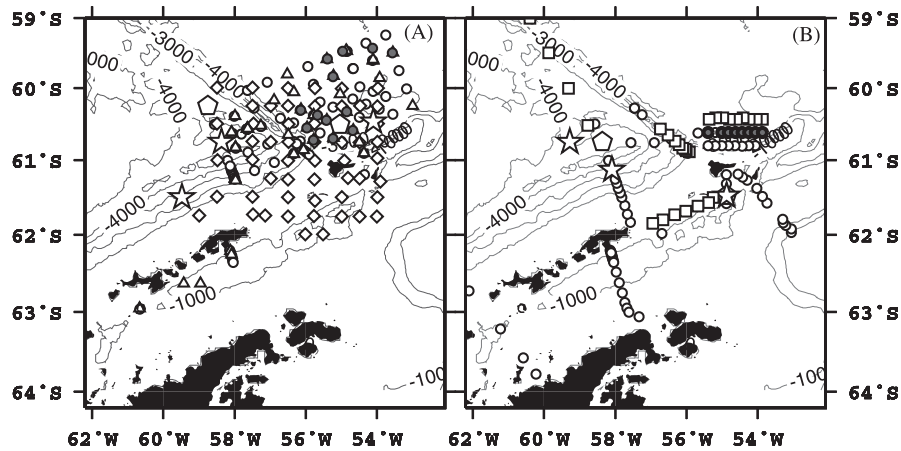


Fig. 2. Station locations and source water points for (A) the LMG0402 and AMLR and (B) NBP0606 cruises. In (A), circles represent LMG0402 CTD stations, triangles represent TMC stations and diamonds represent AMLR CTD stations. In (B), circles represent CTD stations and squares represent XCTD casts. In both panels, stars identify the stations used as source points for the three-source scenario in the OMP analysis and pentagons mark the source points for the two-source scenario. Gray circles mark stations where iron was sampled.

equipped with 11 Niskin bottles. Nutrients were sampled only during Leg 1. Lipsky (2004) provides a full description of the instruments and methods used by the survey.

Two sets of CTD sensors were mounted on the RPSC rosettes and compared against each other at the beginning and end of the cruise in order to check for sensor drift. One set of sensors was used on the TMC rosette during LMG0402 and compared against the RPSC sensors. Because the thermocline waters in the study region are subject to high temporal variability, comparisons of RPSC vs. TMC sensors were done only for the 24 stations for which RPSC and TMC casts were performed within 4 h of each other, and where the casts reached a depth of at least 1000 m. All sensor pair comparisons showed temperature differences within 0.01 °C and salinity differences within 0.01 ppt (Zhou et al., 2010a). In addition to the CTD casts, 36 expendable CTDs (XCTDs) were dropped during NBP0606 but were not included in the analysis due to possible instrument bias.

Dissolved iron concentrations were determined from water samples taken with the TMC rosette at locations indicated by the shaded circles in Fig. 2. The concentrations were originally determined on board ship using the flow injection analysis method and subsequently reprocessed using inductively coupled plasma mass spectrometry (ICP-MS) (Measures et al., 2013). Only a limited amount of data was obtained in the ACC waters with the lowest iron concentrations during LMG0402. Furthermore, iron was not measured during the 2004 NOAA-AMLR survey. In this study, we use the iron profiles to identify a density range corresponding to the subsurface iron peak but, since the iron data are sparse, we do not use iron as a parameter in the OMP analysis. However, other water properties, such as temperature, salinity, oxygen and nutrients, can be used to analyze the distribution of waters originating on the Antarctic shelf (Hewes et al., 2008), which are known to be high in iron throughout the region (Ardelan et al., 2010; Hewes et al., 2008).

The oxygen concentrations measured by the RPSC sensors during LMG0402 and NBP0606 were calibrated by using Winkler titration oxygens from selected rosette bottles. Potential density for each titration was calculated from the CTD data at the depth of the bottle closures, and oxygen values from the titrations were compared against the sensor readings at matching densities during the downcasts. Oxygen samples were not drawn from the bottles mounted on the TMC rosette, so the TMC oxygens were calibrated using only the stations where titrations from an RPSC cast were available for the same location. The AMLR oxygen concentrations were not calibrated on board ship, since no titrations were conducted during the survey.

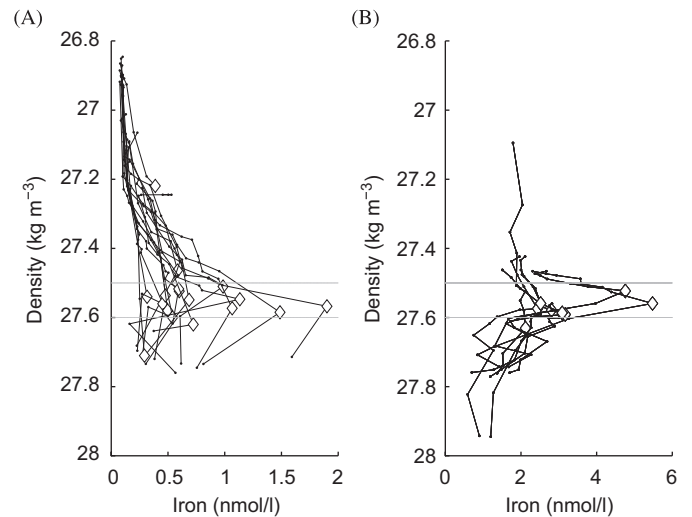


Fig. 3. Profiles of iron concentration vs. density in the Ona Basin for (A) March 2004 (LMG0402) and (B) August 2006 (NBP0606). The $27.5 \leq \sigma_{\theta} \leq 27.6$ density layer is indicated by the gray horizontal lines. Diamonds indicate the iron maximum at each individual station.

2.1. Iron distribution and selection of the density range for OMP analysis

Profiles of iron vs. density for the stations sampled in the Ona Basin during LMG0402 and NBP0606 are shown in Fig. 3. While the LMG0402 concentrations throughout the water column are significantly lower than the NBP0606 values, the highest iron concentrations for both cruises were observed below the mixed layer, in the depth range from 100 to 200 m. For the Ona Basin profiles, the iron maximum for most stations is located at a potential density surface in the range $27.5 \leq \sigma_{\theta} \leq 27.6$, which is the range we selected as the focus for our analysis. The thickness and median depth of this density layer are shown in the top rows of Fig. 4 for LMG0402 and Fig. 5 for NBP0606.

The $27.5 \leq \sigma_{\theta} \leq 27.6$ density range was chosen to be wide enough to include at least one nutrient bottle sample for all stations included in the analysis. However, the nutrient profiles in this range show high gradients that may affect the OMP results once the nutrient values are vertically averaged to compute the OMP inputs. To reduce this effect and better evaluate the vertical consistency of our results, we also examine the density layer

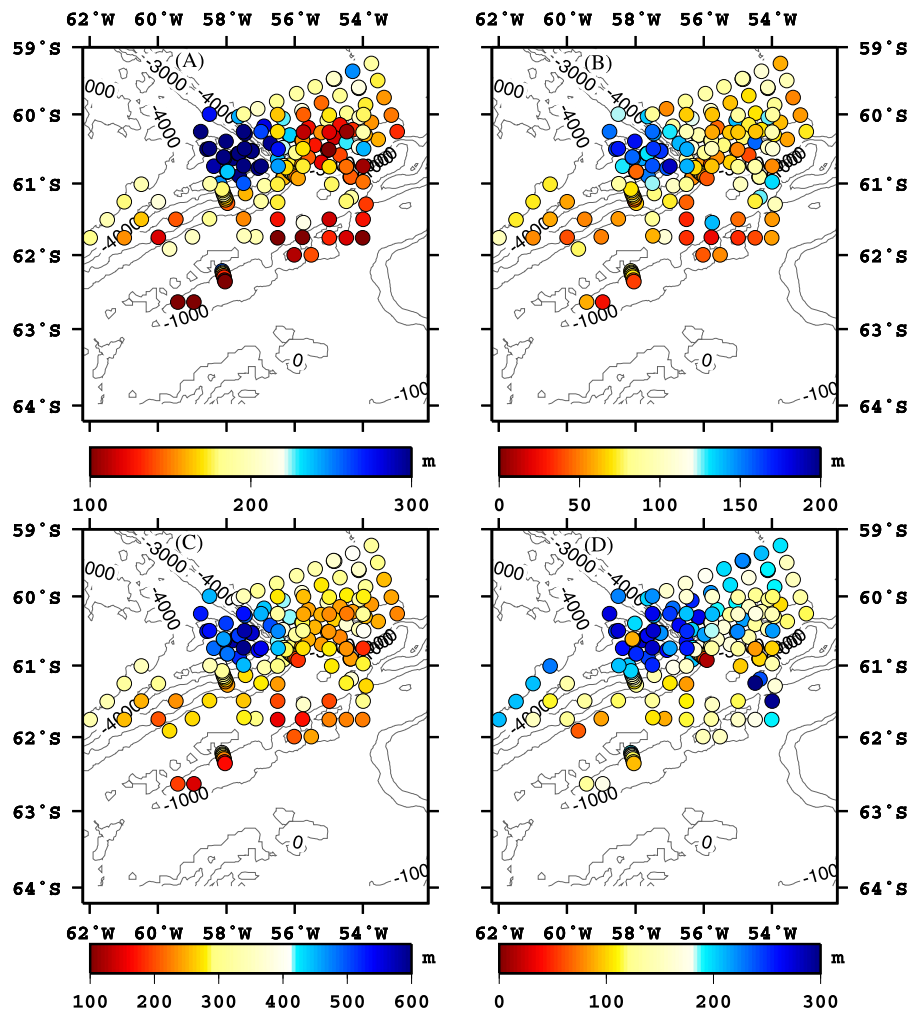


Fig. 4. Top row: median depth (A) and thickness (B) of the $27.5 \leq \sigma_{\theta} \leq 27.6$ density range containing the iron peak for LMG0402. Bottom row: median depth (C) and thickness (D) of the density range $27.6 \leq \sigma_{\theta} \leq 27.7$.

below the iron maximum, defined as $27.6 \leq \sigma_{\theta} \leq 27.7$, where the nutrient gradients are small. The thickness and median depth for this deeper layer are shown in the bottom rows of Fig. 4 for LMG0402 and Fig. 5 for NBP0606.

For both cruises, the two density layers are thicker in the deep waters to the west of the STR than the deep waters to the east. For LMG0402, both layers are thinnest over the continental shelf on both sides of the ridge, and become thicker away from the shelf. For NBP0606, the layers are thinnest for shelf transects A and C (Fig. 2B), where the end point stations for the shelf waters used in our OMP analysis are defined.

2.2. Selecting source water for OMP analysis

Optimal Multiparameter analysis, as developed by Tomczak and Large (1989) and described in detail in Appendix A, is based on the assumption that observed water properties at a hydrographic station are the result of mixing among two or more “source waters”. Usually the source waters are assumed to be linear combinations of two or more sea water types (SWTs), whose physical and chemical properties are known (Tomczak and Large, 1989). The input values for the OMP computation are then determined by linear regression of all parameters against temperature. By limiting our analysis to a vertically narrow isopycnal layer, we were able to define each of our source waters as a single SWT. This approach allowed us to determine the input values directly

from observations by taking measurements of each parameter at selected end point stations and averaging them vertically within the layer where the analysis would be performed.

Appropriate definition of source water properties is crucial to achieving physically meaningful results from OMP. To identify the stations that best represent the source waters for our region, we compared the temperature–salinity (TS) profiles from the CTD casts in our data set against the characteristic TS properties of the water masses in Drake Passage (Hofmann et al., 1996; Whitworth et al., 1994; Zhou et al., 2010b). We considered potential end points in the ACC, the Bransfield Strait, and on the continental shelf, with additional consideration given to differences between the shelf waters to the east and west of the STR.

Fig. 6 shows the TS profiles for stations used to select potential OMP end points for summer (Fig. 6A) and winter (Fig. 6B). Profiles plotted in red represent stations located north of the SACC and east of the STR, where the ACC flow can be expected to dominate. All stations in both years show the typical CDW profile, with Upper Circumpolar Deep Water (UCDW) profile below the 27.2 isopycnal, consistent with previous sections across Drake Passage (Brandon et al., 2004). Above the 27.2 isopycnal, the LMG0402 stations show the warmer and slightly fresher Antarctic Surface Water (ASW) layer that is not present during NBP0606, as is consistent with surface warming during the summer months.

The shelf water profiles in Fig. 6 are plotted in green for stations west of the STR and blue for stations to the east. During

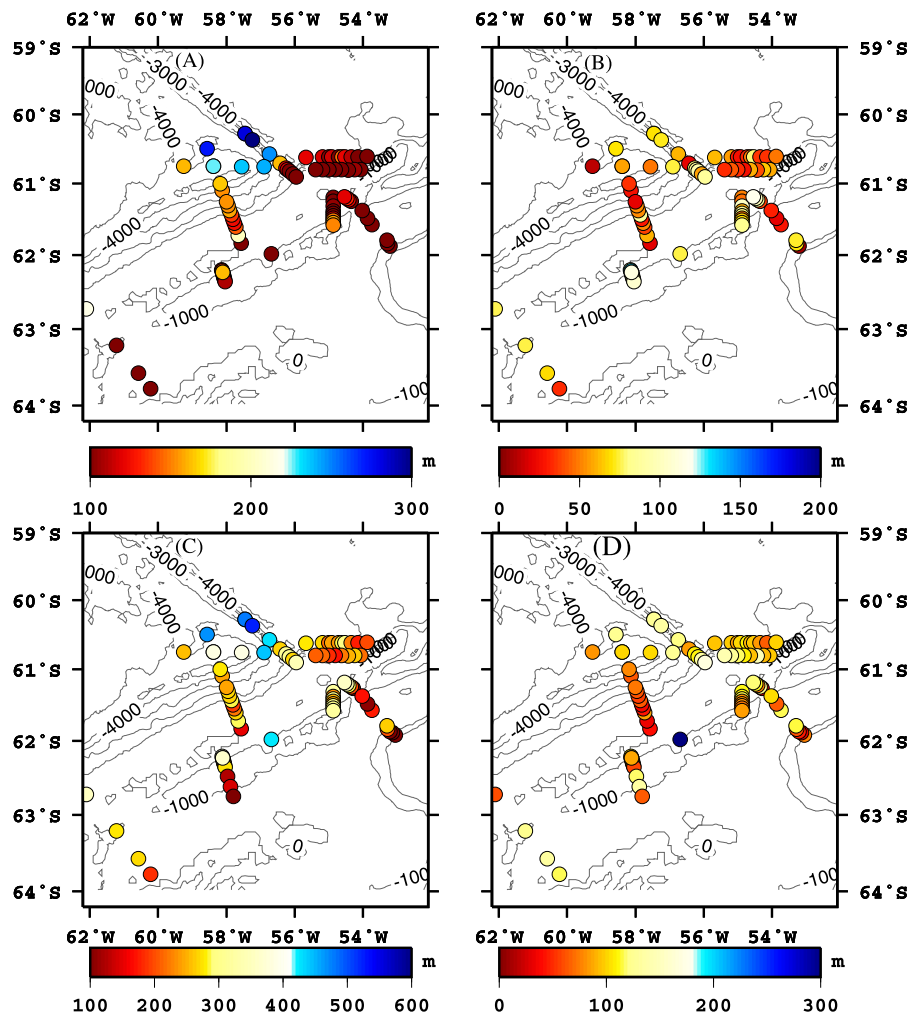


Fig. 5. Top row: median depth (A) and thickness (B) of the $27.5 \leq \sigma_{\theta} \leq 27.6$ density range containing the iron peak during NBP0606. Bottom row: median depth (C) and thickness (D) of the density range $27.6 \leq \sigma_{\theta} \leq 27.7$.

LMG0402, the western stations fall into two distinct clusters. One cluster shows the characteristic CDW profile, closely overlapping with the ACC profiles above the 27.2 isopycnal, but becoming consistently colder than the ACC for $\sigma_{\theta} > 27.2$, consistent with local cooling of the CDW. The other cluster shows colder, saltier shelf waters consistent with the intrusion of BW into the shelf waters around the South Shetland Islands. However, the TS profiles in the second cluster could not be easily distinguished from the profiles east of the STR. For the NBP0606 profiles, the differences between the two clusters of the western shelf stations are less distinct, and the coldest of the western shelf stations once again show significant overlap in water properties with the eastern shelf stations.

Profiles from the Bransfield Strait are plotted in magenta in Fig. 6. For LMG0402, the BW profiles are similar to the SW profiles sampled east of the STR, but with temperatures up to 0.5 °C colder than SW in our chosen density range. During NBP0606, when the Bransfield Strait stations were sampled in a high-resolution transect across the entire strait, the TS profiles overlap with the SW profiles both east and west of the STR, reflecting the difference in water properties between the northeastward flow of the Bransfield Current along the southern shelf of the South Shetland Islands and the southwestward countercurrent in the southern part of the strait (Hofmann et al., 1996; Zhou et al., 2002, 2006).

Temperature and salinity alone suggest two potential source waters for OMP analysis, one representing the ACC and one

representing all shelf waters (SW) in the study region. However, circulation studies based on drifter tracks and ADCP measurements (Niiler et al., 1991; Thompson et al., 2007, 2009; Whitworth et al., 1994; Zhou et al., 2002) suggest that the shelf waters upstream of the STR are modified by Bransfield Water, while the shelf waters downstream are influenced by outflow from the Weddell Sea. Therefore, the upstream and downstream shelf waters can potentially represent two separate source waters, with ACC as the third source. OMP analysis allows for the inclusion of other parameters, such as nutrients, oxygen and potential vorticity, which may help distinguish waters that have similar TS properties but originate from different sources. While nutrient concentrations are affected by biogeochemical processes and cannot be assumed to be conserved during mixing, Karstensen and Tomczak's (1998) extension of the original OMP method accounts for these changes through the use of Redfield ratios, further explained in Appendix A. The nutrient data allow us to make further distinction between the shelf waters to the east and west of the STR. We will refer to the SW on the western side of the STR as SW1 and to the SW on the eastern side as SW2. The additional parameters also allow us to test the suitability of BW as an additional source water, both as a potential fourth source and as a replacement for either SW1 or SW2 in a three-source scenario.

The potential vorticity (PV) for our analysis was computed as

$$PV = \frac{N^2 f}{g}, \quad (1)$$

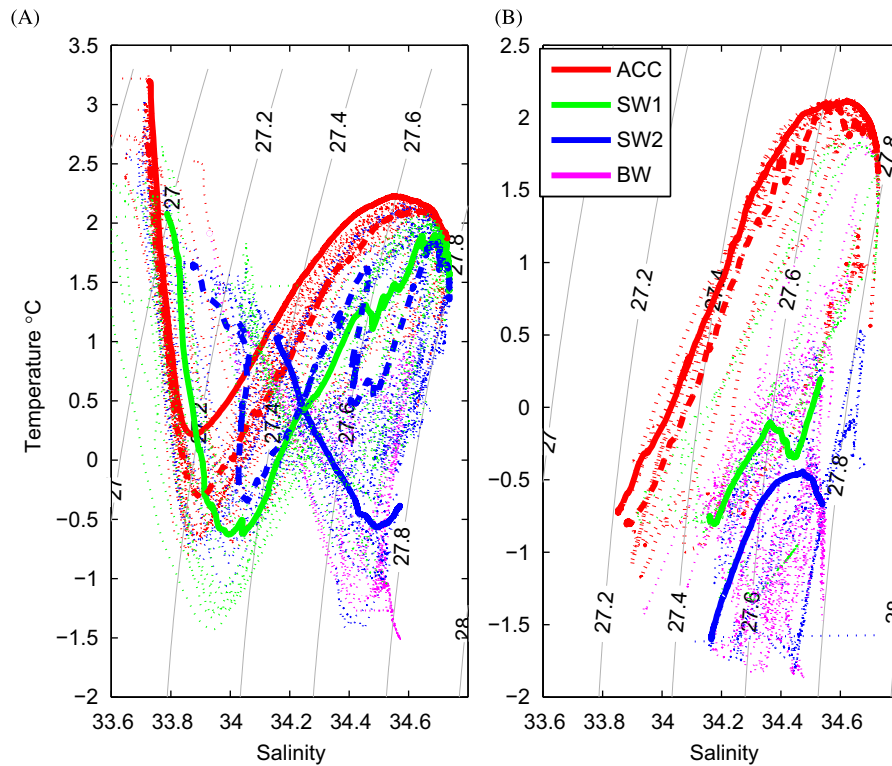


Fig. 6. Temperature and salinity profiles for stations used to determine source water properties for OMP analysis. For the three-source scenario, solid red lines represent the stations chosen to represent the source waters for (A) LMG0402 and (B) NBP0606. Solid green lines represent the SW1 source water stations and solid blue lines represent the SW2 stations. For the two-source scenarios, dashed lines represent the stations chosen for ACC and SW. During NB060, the same station was selected to represent SW2 and SW in both scenarios. Dotted lines in each color represent the other stations sampled within the same source water. (For interpretation of the references to color in this figure caption, the reader is referred to the web version of this article.)

Table 1
Definitions of source water end points used for the three-source OMP analysis.

Source water	Latitude	Longitude	Temperature (°C)	Salinity (psu)	O ₂ (μmol/kg)	PO ₄ (μmol/kg)	NO ₃ (μmol/kg)	Si (μmol/kg)	Pot. Vort.
27.5 ≤ σ_θ ≤ 27.6, LMG0402+AMLR									
ACC	−60.52	−57.26	1.84	34.46	189	2.4	35.1	54.5	0.10
SW1	−61.20	−58.03	1.56	34.44	228	2.7	51.4	115.3	0.10
SW2	−60.51	−58.70	1.37	34.42	208	2.2	33.1	69.1	0.21
27.6 ≤ σ_θ ≤ 27.7, LMG0402+AMLR									
ACC	−60.53	−57.26	2.08	34.61	171	2.4	34.6	74.9	0.06
SW1	−61.20	−58.03	1.80	34.59	175	2.3	34.3	70.3	0.10
SW2	−60.51	−58.70	1.33	34.54	191	2.3	34.7	75.3	0.08
27.5 ≤ σ_θ ≤ 27.6, NBP0606									
ACC	−60.50	−58.56	0.81	34.38	217	1.9	31.8	71.7	−0.18
SW1	−61.61	−57.73	0.49	34.36	297	1.9	33.9	75.7	−0.88
SW2	−61.25	−54.88	−0.55	34.26	288	1.7	32.6	77.2	0.06
27.6 ≤ σ_θ ≤ 27.7, NBP0606									
ACC	−60.50	−58.56	2.07	34.61	173	2.2	34.6	79.2	0.07
SW1	−61.61	−57.73	0.25	34.43	264	2.0	31.2	75.4	0.08
SW2	−61.25	−54.88	−0.37	34.42	265	1.8	35.0	87.3	−0.02

where N is the buoyancy frequency, f is the Coriolis frequency, and g is the gravitational acceleration. As seen in Figs. 4 and 5, the density layers covered in our analysis are thickest in the north-west portion of our sampling region, where the CDW TS properties dominate, and thinnest on the shelf. The resulting difference in potential vorticity helps us to further distinguish the ACC waters from the shelf waters.

To select appropriate stations for defining our source waters, we defined a parameter space of seven dimensions: temperature, salinity, oxygen, phosphate, nitrate, silicate and PV. At each station, a seven-element vector of these parameters was

computed by vertically averaging the values of each parameter over the $27.5 \leq \sigma_{\theta} \leq 27.6$ density layer. Each vector was then normalized following Karstensen and Tomczak's (2005) method as described in Eq. (A.2) in Appendix A. To ensure that the results of the OMP analysis most fully describe the water composition in our region, it is desirable to select stations whose property vectors most fully span our parameter space to represent our source waters. If using two source waters, this criterion can be satisfied by choosing two stations whose coordinate vectors place them farthest apart in the parameter space. To select three source waters, we can view them as points defining a triangle in the

parameter space, and select the three stations whose coordinate vectors span the largest triangle area. By extension, an ideal four-source scenario would use four points defining a solid with maximum volume in the parameter space. However, preliminary tests with a four-source scenario showed that it did not represent the mixing in the region as well as a three-source scenario, and the possibility of a fourth source water was not explored in greater detail.

The locations and averaged water properties of the source water stations selected for the two-source and three-source scenarios are shown in Tables 1 and 2. The profiles for these stations are plotted as solid and dashed lines in Fig. 6.

2.3. Sensitivity analysis

To obtain a quantitative measure of the robustness of our computed source water distributions, we examined the sensitivity of our results to random variations in the source water definitions. A total of 100 iterations of a Monte Carlo simulation were performed. For each iteration, random perturbations for each parameter – temperature, salinity, oxygen and nutrients – were generated from a zero-mean Gaussian distribution with the same standard deviation as the measured parameter within each source water. A standard deviation of the difference between the simulated scenarios and the unperturbed scenario was computed for the fractional contribution

from each source water at every station, as well as a mean standard deviation for the entire region. Standard deviations for the mass residuals at each station were also computed.

As an alternative sensitivity estimate, we also examined the standard deviations of each source water distribution within the isopycnal layer prior to averaging. The resulting sensitivity values (not shown) were smaller than the values given by the Monte Carlo method for 85% of all stations. Since this estimate does not account for measurement bias or for the high degree of correlation likely to exist for vertically adjacent points within an isopycnal, we chose the Monte Carlo method as a more complete measure of the sensitivity of our results.

3. Results and discussion

We performed the OMP analysis for all CTD stations, using as inputs the averaged temperature, salinity, nutrient and PV values for the density range illustrated in the top row panels of Figs. 4 and 5. The source water distributions were computed twice, once for the two-source and once for the three-source scenario. Changing the number of source waters in the analysis affects the residuals computed by OMP. Therefore the two-source and three-source scenarios cannot be meaningfully compared based on the residuals. Instead, we compared the scenarios by calculating a chi-square (χ^2) estimator (Press et al., 1986) for the

Table 2
Definitions of source water end points used for the two-source OMP analysis.

Source water	Latitude	Longitude	Temperature (°C)	Salinity (psu)	O ₂ (μmol/kg)	PO ₄ (μmol/kg)	NO ₃ (μmol/kg)	Si (μmol/kg)	Pot. Vort.
27.5 ≤ σ ≤ 27.6 LMG0402+AMLR									
ACC	−60.25	−58.70	1.80	34.45	189	2.2	31.9	54.5	0.10
SW	−60.51	−55.04	1.37	34.42	208	2.2	33.1	69.1	0.22
27.6 ≤ σ ≤ 27.7, LMG0402+AMLR									
ACC	−60.25	−58.70	2.08	34.61	171	2.4	34.6	74.9	0.06
SW	−60.51	−55.04	2.03	34.62	198	2.4	44.3	93.6	0.06
27.5 ≤ σ ≤ 27.6, NBP0606									
ACC	−60.75	−58.37	1.69	34.45	189	2.2	37.7	64.8	0.11
SW	−61.32	−54.88	−1.24	34.23	316	1.9	26.1	77.9	0.13
27.6 ≤ σ ≤ 27.7, NBP0606									
ACC	−60.75	−58.37	2.00	34.60	173	2.2	30.0	74.1	−0.79
SW	−61.25	−54.88	−0.53	34.42	276	1.8	34.6	77.3	0.09

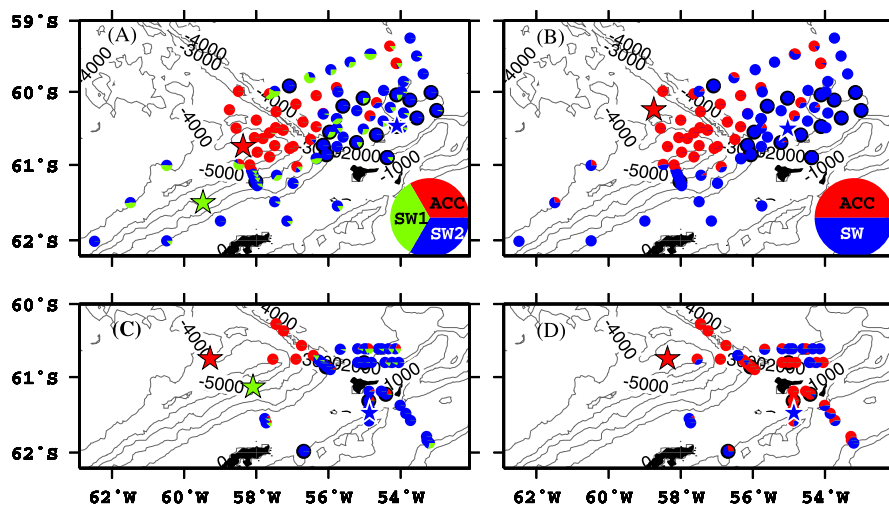


Fig. 7. Source water distributions along the $27.5 \leq \sigma_{\theta} \leq 27.6$ isopycnal computed with OMP analysis during LMG0402 (A and B) and NBP0606 (C and D). The pie charts show station locations and stars show the locations of source point stations. The source waters for the three-source scenario (A and C) are ACC water (ACC), Shelf Water 1 (SW1), and Shelf Water 2 (SW2). The source waters for the two-source scenario (B and D) are ACC and Shelf Water (SW). Pie charts circled in black represent stations where Monte Carlo analysis produced a root-mean-square difference of more than 0.05 from the unperturbed case.

standard deviation of individual parameters at all stations, and computed the probability of exceeding a given χ^2 value with random data. The details of the method are given in Appendix B.

The resulting source water distributions are illustrated by the pie charts in Fig. 7, and the spatially averaged results of the Monte Carlo sensitivity analysis for the entire study region are summarized in Table 4. The distributions for individual LMG0402 and AMLR stations are shown in Fig. 7A for the three-source scenario and Fig. 7B for the two-source scenario. The same scenarios for NBP0606 are illustrated in Fig. 7C and D. Stars indicate the locations of the stations used to define the source waters for each scenario. The different criteria for two-source and three-source selections, as described in Section 2.2, resulted in different stations representing the ACC source water in the two scenarios. For comparison, we also performed the analysis using the same ACC definition for both scenarios. The results for individual stations (not shown) did not differ from the results in Fig. 7 by more than the standard deviation computed from the sensitivity analysis described in Section 2.3.

Upstream of the STR, where the density layer is thickest, the distributions for both summer and winter show the ACC water as the dominant water mass in the region, with little or no shelf water present in the stations north of the 2500 m bathymetry contour. This part of the region is also characterized by low iron (Ardelan et al., 2010; Hewes et al., 2008; Martin et al., 1990) and low Chl-a (Fig. 1B). Downstream of the STR, where the Chl-a levels are elevated, the three-source scenario shows the shelf waters dominating the water composition, with 60% of LMG0402 stations and 67% of NBP0606 CTD stations in the three-source scenario showing ACC contributions of less than 5% (Fig. 7A and C). This distribution is consistent with Zhou et al.'s (2010a) conclusion that the ACC flow east of the STR is redirected to the northeast by conservation of potential vorticity.

One unexpected result of the analysis was the inconsistency between the two-source and three-source scenarios for NBP0606, as seen in Fig. 7C and D. The two-source scenario shows ACC water present throughout the region, including the shelf stations on both sides of the STR. A possible reason for the inconsistency between the two- and three-source scenarios for NBP0606 comes as a result of the averaging of the input parameters within a density layer. For NBP0606, the nutrient profiles for the selected source waters show high gradients in the $27.5 \leq \sigma_\theta \leq 27.6$ density layer, with overlapping values between the ACC and shelf water profiles. Averaging over the density layer produces values for ACC,

SW and SW1 that cannot be easily distinguished. The similarities in the source waters are reflected in the higher uncertainties produced by the Monte Carlo analysis for the NBP0606 data (Table 4). A clearer distinction between the ACC and shelf waters can be seen on the $27.6 \leq \sigma_\theta \leq 27.7$ isopycnal (Fig. 8C and D), where the source water nutrient profiles do not overlap, and the gradients are smaller.

The three-source scenarios for both summer and winter show both SW1 and SW2 present upstream and downstream of the STR, with SW1 properties dominating. However, our sensitivity analysis indicates that the stations dominated by mixing between SW1 and SW2 show the highest sensitivity to small perturbations in the source water definitions, suggesting that the properties of SW1 and SW2 are not sufficiently different to be well-distinguished by the OMP analysis. The χ^2 estimator test indicates a probability difference of less than 0.5% between the two-source and three-source scenarios, and the ACC contributions between the two scenarios showed no statistically significant changes, with differences at all stations being smaller than the standard deviations computed in our sensitivity analysis. The similarity between the two scenarios suggests intermixing among shelf waters in the sampling region, with Weddell Sea waters influencing the hydrographic properties at all shelf stations. Such mixing is consistent with past hydrographic (Niiler et al., 1991; von Gyldenfeldt et al., 2002) and drifter (Zhou et al., 2002) studies, which indicate that some northward-flowing Weddell Sea waters turn southwestward at the tip of the Antarctic Peninsula and intrude into the Bransfield Strait and the shelf break around the South Shetland Islands.

The distributions for the three-source scenarios that included BW as a source point (not shown) were similar to the three-source distribution shown in Fig. 7, with a mixture of BW and SW dominating the circulation east of the STR. However, both the sensitivity analysis described in Section 2.3 and the χ^2 estimator computed following the method in Appendix B indicate that the waters in the Ona Basin are more accurately represented as a combination of ACC and shelf waters only, with BW affecting the circulation primarily through its influence on the shelf waters west of the STR.

Distribution of water properties in the ocean is affected by stirring, which redistributes properties through advection while maintaining the presence of gradients, and by mixing, which decreases the gradients through diffusion (Eckart, 1948). Abraham et al. (2000) have demonstrated the importance of horizontal stirring in the

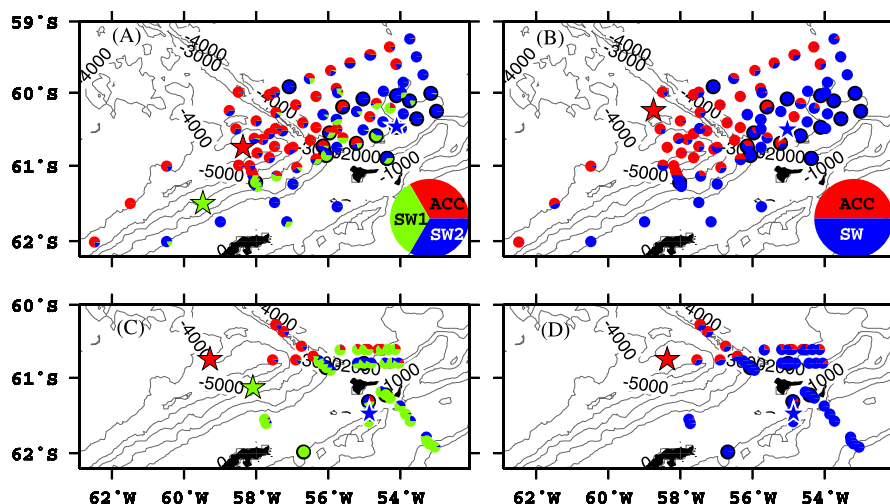


Fig. 8. Source water distributions along the $27.6 \leq \sigma_\theta \leq 27.7$ isopycnal computed with OMP analysis using only CTD stations during LMG0402 (A and B) and NBP0606 (C and D). Symbols and colors are as in Fig. 7. (For interpretation of the references to color in this figure caption, the reader is referred to the web version of this article.)

development and sustainment of an iron-fertilized bloom. The OMP-derived distributions in Fig. 7 show that within the Ona Basin, in the central part of our study region, the water composition varies from station to station. Adjacent stations are frequently dominated by different source waters. Using Argo data, Barré et al. (2008) found similar patchiness of potential temperature, salinity and σ_θ distributions in the same region. Such variable distribution near the ridge is consistent with a filamented structure that could be caused by advective stirring. Farther downstream, the easternmost LMG0402 stations show a more uniformly mixed water composition dominated by shelf waters, suggesting that the waters are retained within the basin long enough for the stirring to lead to mixing, homogenizing the water properties as the water advects downstream. Such a scenario is consistent with Argo floats becoming trapped in the basin for periods ranging from 6 to 20 months between 2002 and 2006 (Barré et al., 2008). For NBP0606, the stations at the eastern edge of the study region are too few and too closely spaced to determine if homogenized mixing has taken place.

The source water distributions along the $27.6 \leq \sigma_\theta \leq 27.7$ density layer, shown in Fig. 8, indicate that the source water distributions for LMG0402 are vertically consistent over different density ranges, while the distributions for NBP0606 show a clearer distinction between ACC and shelf waters, with ACC waters present only in the northernmost stations. These distributions were calculated using the same end point station locations as the iron peak layer. For the three-source scenario, the distributions for NBP0606 (panel C) are largely the same as in the iron maximum layer, with a slightly greater presence of SW1 in the Ona Basin, and ACC water still dominant west of the STR. The LMG0402 distribution (panel A) shows a smaller presence of ACC water throughout the region, but retains the filamented distribution in the Ona Basin with homogenized mixing in the east. Distributions computed with endpoints optimized for the $27.6 \leq \sigma_\theta \leq 27.7$ layer (not shown) slightly increase the ACC concentrations west of the STR, but do not significantly affect the results for the Ona Basin. The two-source distribution for LMG0402 (panel B) is similar to the distribution for the $27.5 \leq \sigma_\theta \leq 27.6$ density layer, while the two-source distribution for NBP0606 (panel D) shows a higher proportion of ACC waters, especially for stations where SW1 is dominant in the three-source scenario, suggesting a stronger winter influence of CDW in this density range on the shelf waters west of the STR.

The extended OMP analysis for the two-source scenario on the $27.5 \leq \sigma_\theta \leq 27.6$ isopycnal produced ΔP values of $0.014 \pm 0.004 \mu\text{mol/kg}$ for LMG0402 and $0.20 \pm 0.014 \mu\text{mol/kg}$ for NBP0606. The higher value for NBP0606 runs counter to the expectation that nutrient changes should be small in winter, when phytoplankton growth is low. However, physical processes such as winter upwelling and deep-penetrating air–sea interactions may also affect wintertime nutrient concentrations. In addition, the higher uncertainties in the NBP0606 source water distributions suggest that the ACC and SW properties are less distinct in winter than in summer. Since temperature and salinity are weighted higher than nutrients in our wintertime analysis, computational inconsistencies in the OMP analysis may be reflected more strongly in the ΔP values.

While the winter distributions shown in Figs. 7 and 8 are consistent with the summer distribution in showing the increased presence of shelf waters in the Ona Basin compared to the ACC-dominated waters to the west of the STR, the CTD casts during NBP0606 did not sample far enough off-shore to determine if the filamented distribution seen in the summer months is still present in winter.

4. Summary

In this study, we have used CTD data from multiple surveys to perform an OMP analysis of the source water distribution in the

southern Drake Passage during the summer of 2004 and the winter of 2006. The extended version of the OMP analysis was used, incorporating Redfield ratios to partially account for the biogeochemical changes. The results give us the means to assess the horizontal distribution of iron-rich shelf waters in our study region.

Adjacent stations near the STR in the Ona Basin show very different source water compositions, consistent with a filamented distribution created by advective stirring. Farther downstream, the source water distribution becomes more uniform, suggesting that the waters in the basin are retained long enough for the stirring to eventually lead to homogeneous mixing. Satellite-derived Chl-a images (Kahru et al., 2007) also demonstrate filamentation, with adjacent strands of high and low Chl-a found in eddies and frontal zones.

While the shelf waters near the South Shetland Islands are geographically separated from the shelf waters near the Weddell Sea (Hofmann et al., 1996; Zhou et al., 2010b), treating the two as separate shelf water sources did not produce statistically significant improvements in either the χ^2 estimator or the sensitivities computed from the Monte Carlo simulation described in Section 2.3. The similarities between the results of the two-source and three-source scenarios for both density ranges analyzed during LMG0402 and for the $27.6 \leq \sigma_\theta \leq 27.7$ range during NBP0606 suggest that the shelf waters are not sufficiently distinct in their TS and nutrient properties to justify treating them as separate source waters for the purposes of our analysis. By contrast, the χ^2 and sensitivity results for scenarios that include the Bransfield Strait indicate that BW does not directly contribute to the mixing in the Ona Basin but instead influences the source water distributions in the basin only indirectly, through its influence on the shelf waters.

The distributions shown in Figs. 7 and 8 indicate that in the density range where iron concentration is highest, shelf waters from both east and west of the STR flow into the Ona Basin. Previous studies of circulation in the region (Barré et al., 2008; Brandon et al., 2004) indicate the presence of persistent deep mesoscale eddies that trap water in the basin. In Barré et al.'s (2008) study, Argo floats released in March 2002 and December 2003 remained in the basin for periods ranging from six months to two and a half years. Such long retention times, combined with the off-shore advection of shelf waters suggested by our analysis, would allow for a build up of high iron concentrations below the mixed layer in the Ona Basin. A companion paper, Frants et al. (2013), explores some of the physical mechanisms that may enable the iron from the subsurface maximum to reach the euphotic zone.

Acknowledgments

The authors thank James Swift of Scripps Institution of Oceanography, Christian Reiss of Southwest Fisheries Science Center, William T. Hiscock of the Universität Bern, Switzerland, the crews of the *R/V Laurence M. Gould* and the *R/V Nathaniel B. Palmer*, the members of the AMLR survey, and the employees of the Raytheon Polar Services Company.

The funding for this research was provided by the National Science Foundation, Grants nos. ANT0444134, ANT0948338, OCE0957342 and OCE0622740.

Appendix A. OMP analysis

A.1. The method

Optimal Multiparameter analysis was introduced by Tomczak and Large (1989). It is an extension of the multiparameter method

originally developed by Tomczak (1981), which in itself is an extension of temperature–salinity diagram analysis. The method allows for the use of hydrographic properties other than temperature and salinity to determine quantitatively the mixing ratios of n water types from a system of m linear equations. It has been used to evaluate water mass properties both in the Southern Ocean (Budillon et al., 2003; Tomczak and Liefink, 2005) and in other regions (e.g. Tomczak and Large, 1989; Tomczak and Poole, 1999). This section provides a brief summary of the method.

Consider a situation in which n source waters contribute to a mixture of water observed at a hydrographic station. Assume the existence of a minimum of $m-1$ oceanic parameters (such as temperature, salinity or oxygen), where $m > n$. The values of these parameters are measured both for the source water end point stations and for the other hydrographic stations. Water properties are assumed to be conserved during mixing. An additional mass balance constraint is created by requiring that some mixture of the source waters fully describe the water at the point of observation. The relative contributions of the n source waters at the observation point can then be represented by the linear system of conservation equations

$$\mathbf{G}\mathbf{x} - \mathbf{d} = \mathbf{r}, \quad (\text{A.1})$$

where \mathbf{G} is an $m \times n$ matrix containing the parameter values for the source waters, \mathbf{d} is an m -element vector containing the observed parameter values for the mixed water, \mathbf{x} is an n -element vector containing the relative contributions of the source waters to the mixing, and \mathbf{r} is the m -element residual vector. The last line of \mathbf{G} and the last element of \mathbf{d} are set to 1 to represent the mass balance constraint. Traditionally, this final constraint is used as a measure of the uncertainty of the result, with mass balance residuals of 0.05 or less considered acceptable (Budillon et al., 2003; Tomczak, 1981; Tomczak and Large, 1989; Tomczak and Poole, 1999). The system is solved as an overdetermined least squares problem, minimizing $\mathbf{r}^T \mathbf{r}$, subject to the constraint that all elements of \mathbf{x} must be nonnegative.

Before the system of equations in A.1 can be solved, the values in \mathbf{G} must be normalized in order to make parameters of different units comparable. We follow Karstensen and Tomczak's (2005) method of computing the normalized matrix \mathbf{G}' where

$$G'_{ij} = (G_{ij} - \bar{G}_j) / \sigma_j, \quad (\text{A.2})$$

where G_{ij} is the value of parameter j for source water i , G'_{ij} is the normalized value, \bar{G}_j is the mean value of the parameter, and σ_j is the standard deviation.

In order to account for the biogeochemical changes in the source waters, we followed Karstensen and Tomczak's (1998) extension of the original OMP method by adding another column $r_{para} \Delta P$ to the left-hand side of Eq. (A.1). The new column contains the Redfield ratios (Redfield et al., 1963) for oxygen, nitrate, phosphate and silicate, multiplied by the new unknown variable ΔP representing the change in phosphate (Karstensen and Tomczak, 2005). For temperature, salinity and mass balance, corresponding elements in the new column are set to 0. Eq. (A.1) can then be rewritten as

$$\mathbf{G}_{ext} \mathbf{x}' - \mathbf{d} = \mathbf{r}, \quad (\text{A.3})$$

where $\mathbf{G}_{ext} = [\mathbf{G} \mathbf{r}_{para}]$ and $\mathbf{x}' = [\mathbf{x} \Delta P]^T$. In this new equation, \mathbf{G}_{ext} becomes a $m \times n+1$ matrix, requiring $m > n+1$ in order to ensure that the system remains overdetermined.

The canonical N:P:O₂ ratios suggested by Redfield et al. (1963) are 16:1:–138. Hoppema and Goeyens's (1999) analysis of N:P ratios in the western Weddell Sea indicated that the canonical values apply in Antarctic surface waters. Silva et al. (1995) showed similar mean values for the N:P ratio in the waters around Elephant Island, but

found that mean Si:P values varied from 23:1 to 43:1, depending on depth and region of observation. Our own calculations, based on averaging the ratios for stations within the Ona Basin, produced Si:N:P:O₂ of 29:15:1:–156 for LMG0402 and 41:18:1:–184 for NBP0606. The results discussed in Section 3 are based on our calculated ratios for each cruise. Replacing the O₂ and N ratio with canonical Redfield values produced no statistically significant differences in the source water distributions or in the computed values of ΔP .

Due to variations in measurement accuracy and spatial and temporal variability of the observed parameter values, a diagonal weight matrix \mathbf{W} of dimension $m \times m$ is introduced. The full solution of the OMP analysis is then found by minimizing

$$(\mathbf{G}_{ext} \mathbf{x}' - \mathbf{d})^T \mathbf{W}^T \mathbf{W} (\mathbf{G}_{ext} \mathbf{x}' - \mathbf{d}) = \mathbf{r}^T \mathbf{r}. \quad (\text{A.4})$$

Usually, the source waters in OMP analysis are assumed to be linear combinations of two or more sea water types (SWTs), whose physical and chemical properties are known (Tomczak and Large, 1989). The values of \mathbf{G} are then determined by linear regression of all parameters against temperature. By limiting our analysis to a vertically narrow isopycnal layer, we were able to define each of our source waters as a single SWT. This approach allowed us to determine the values of \mathbf{G} directly from observations by taking measurements of each parameter at selected end point stations and averaging them vertically within the layer where the analysis would be performed.

A.2. Determining the weights

In OMP analysis, the weight matrix \mathbf{W} is usually constructed so that the mass balance equation is assigned the highest weight among all the property conservation equations, and the mass balance residuals provide an objective indicator of the quality of the solution (Tomczak, 1981). In an ideal case, in which there is no measurement error, and the source waters specified in the input matrix \mathbf{G} fully represent all of the waters that have been mixed to form the water at a given station, the last element of \mathbf{r} would be equal to zero. Stations with high mass residuals may have water from other sources contributing to the mixing, or may be subject to non-linear processes that are not well-described by the linear model used in OMP analysis. Therefore, we follow Tomczak and Poole (1999) and focus our discussion on stations where the mass residuals are less than 0.05.

To obtain \mathbf{W} for our analysis, we adapted the method originally described by Tomczak and Large (1989), which is based on relating the variance of each input parameter among the source waters to the variance of the same parameter within each source water. We define σ_j as a measure of how well parameter j is able to resolve the differences among n water masses:

$$\sigma_j = \sqrt{\frac{1}{n} \sum_{i=1}^n (G_{ij} - \bar{G}_j)^2}, \quad (\text{A.5})$$

where G_{ij} represents the element of \mathbf{G} corresponding to the value of parameter j in water mass i and \bar{G}_j is the mean value of parameter j at the end points.

We then calculated the source water variances δ_j using the TS-diagrams in Fig. 6 to determine which stations were most likely sampled within the same source water. We computed the mean value of each parameter for each group of stations within the layer where the analysis was to be performed, and computed the variance of the means. The largest of the δ_j values among our n source waters is defined as δ_{jmax} . The weights are then

calculated as

$$W_j = \sigma_j^2 / \delta_{jmax}. \tag{A.6}$$

The weights computed for each parameter from the resulting variances are summarized in Table 3. Since OMP does not provide a straightforward method for assigning weights to the mass balance equation, which is not based on any measurements (de Brauwere et al., 2007; Tomczak and Large, 1989), we followed the usual practice (Tomczak and Large, 1989; You and Tomczak, 1993) and assigned the largest of our calculated weights to the mass balance. As an alternative method, we also performed our analysis with weights based on the inverse variances of individual parameter measurements, as is typically done for least-squares fitting methods. While distributions at individual stations were affected by the resulting changes in weights, the resulting spatial distributions of SWT percentages and mass balance residuals remained consistent with the conclusions we present in Section 3. We selected Tomczak and Large's (1989) method as being more physically meaningful, since it takes into account the variability of properties among the different water masses as well as the variability within each mass.

The high weight assigned to Si in the three-source scenario for LMG0402 introduces a potential source of error, since the Si:N ratio can vary spatially due to varying iron availability in the study region (Takeda, 1998; Timmermans et al., 2004). The increased error may provide an additional reason why the two-source scenario produces smaller residuals and lower uncertainties in the source water distribution.

Appendix B. Computing chi-square estimator to assess the optimal number of source waters

The chi-square distribution for the output of OMP analysis for a normally distributed variable *r* can be defined as

$$\chi^2 \equiv \sum_{i=1}^m \left(\frac{r_i}{\sigma_i} \right)^2, \tag{B.1}$$

Table 3
Weights used for OMP analysis in summer 2004 (LMG0402) and winter 2006 (NBP0606).

Parameter	Three-source		Two-source	
	LMG0402	NBP0606	LMG0402	NBP0606
Temperature	10	10	9	9
Salinity	10	11	7	13
Oxygen	7	25	7	15
Phosphate	16	4	2	2
Nitrate	8	3	6	3
Silicate	17	4	2	1
Pot. vorticity	11	19	19	14

Table 4
Spatially averaged standard deviations of source water distributions, computed from a 100-iteration Monte Carlo simulation. The original distributions are given as percentage contributions of each source water to the total mixing at each station, and the percentages in the table represent absolute deviations from the unperturbed case.

Source	LMG0402+AMLR		NBP0606	
	27.5 ≤ σ ≤ 27.6	27.6 ≤ σ ≤ 27.7	27.5 ≤ σ ≤ 27.6	27.6 ≤ σ ≤ 27.7
Water	Isopycnal (%)	Isopycnal (%)	Isopycnal (%)	Isopycnal (%)
ACC	2.2	1.8	5.0	3.9
SW1	2.9	5.1	3.4	5.0
SW2	1.7	4.5	4.0	4.8

where *m* and *r* are defined as in Appendix A and σ_i is the standard deviation of each parameter measured at the station (Press et al., 1986). For values of σ_i at each individual station, we used the standard deviation of that parameter within the source water that dominated at that station, computed using the same method as the standard deviations used to compute the weights in Appendix A.2.

For a given number of degrees of freedom *v*, we compute the probability that the data will not exceed a given value of χ^2 by chance, with higher probability indicating a higher chance that the end point definitions represent the source waters mixing into the region. This probability can be computed as the incomplete gamma function $Q(0.5 \times v, 0.5 \times \chi^2)$ (Press et al., 1986). For the distribution computed here, *v* is the number of stations used in the OMP analysis minus the number of columns in matrix G.

References

Abraham, E.R., Law, C.S., Boyd, P.W., Lavender, S.J., Maldonado, M.T., Bowie, A.R., 2000. Importance of stirring in the development of an iron-fertilized phytoplankton bloom. *Nature* 407, 727–729.

Ardelan, M.V., Holm-Hansen, O., Hewes, C.D., Reiss, C.S., Silva, N.S., Dulaiova, H., Steinnes, E., Sakshaug, E., 2010. Natural iron enrichment around the Antarctic Peninsula in the Southern Ocean. *Biogeosciences* 7, 11–25.

Barré, N., Provost, C., Sennechaël, N., Lee, J.H., 2008. Circulation in the Ona Basin, southern Drake Passage. *J. Geophys. Res.* 113, c04033, <http://dx.doi.org/10.1029/2007JC004549>.

Blain, S., Treguer, P., Belviso, S., Bucciarelli, E., Denis, M., Desabre, S., Fiala, M., Jezequel, V.M., Le Fevre, J., Mayzaud, P., Marty, J.C., Razouls, S., 2001. A biogeochemical study of the island mass effect in the context of the iron hypothesis: Kerguelen Islands, Southern Ocean. *Deep-Sea Res.* 1 48, 163–187.

Boyd, P.W., 2002. The role of iron in the biogeochemistry of the Southern Ocean and Equatorial Pacific: a comparison of in situ iron enrichments. *Deep-Sea Res.* 11, 1803–1821.

Brandon, M.A., Naganobu, M., Demer, D.A., Chernyshkov, P., Trathan, P.N., Thorpe, S.E., Kameda, T., Berezinskiy, O.A., Hawker, E., Grant, S., 2004. Physical oceanography in the Scotia Sea during the CCAMLR 2000 survey, austral summer 2000. *Deep-Sea Res.* 51, 1301–1321.

Budillon, G., Pacciaroni, M., Cozzi, S., Rivaro, P., Catalano, G., Ianni, C., Cantoni, C., 2003. An optimum multiparameter mixing analysis of the shelf waters in the Ross Sea. *Antarctic Sci.* 15, 105–118.

Chisholm, S.W., Morel, F.M.M., 1991. What controls phytoplankton production in nutrient-rich areas of the open sea? *Limnol. Oceanogr.* 36, 1507–1511.

de Baar, H.J.W., de Jong, J.T.M., 2001. Distributions, Sources and Sinks of Iron in Seawater. John Wiley and Sons Ltd., pp. 123–253.

de Baar, H.J.W., de Jong, J.T.M., Bakker, D.C.E., Loscher, B.M., Veth, C., Bathmann, U., Smetacek, V., 1995. Importance of iron for plankton blooms and carbon dioxide drawdown in the Southern Ocean. *Nature* 373, 412–415.

de Brauwere, A., Jacquet, S.H.M., De Ridder, F., Dehairs, F., Pintelon, R., Schoukens, J., Baeyens, W., 2007. Water mass distributions in the Southern Ocean derived from a parametric analysis of mixing water masses. *J. Geophys. Res.* 112, c02021, <http://dx.doi.org/10.1029/2006JC003742>.

Eckart, C., 1948. An analysis of the stirring and mixing processes in incompressible fluids. *J. Mar. Res.* 7, 265–275.

Frants, M., Gille, S.T., Hatta, M., Kahru, M., Measures, C.I., Zhou, M., 2013. Analysis of horizontal and vertical processes contributing to natural iron supply in the mixed layer in Southern Drake Passage. *Deep-Sea Res.* 11 90, 68–76.

Helbling, E.W., Villafane, V., Holm-Hansen, O., 1991. Effect of iron on productivity and size distribution of Antarctic phytoplankton. *Limnol. Oceanogr.* 36, 1879–1885.

Hewes, C., Reiss, C.S., Holm-Hansen, O., 2009. A quantitative analysis of sources for summertime phytoplankton variability over 18 years in the South Shetland Islands (Antarctica) region. *Deep-Sea Res.* 1 56, 1230–1241.

Hewes, C.D., Reiss, C.S., Kahru, M., Mitchell, B.G., Holm-Hansen, O., 2008. Control of phytoplankton biomass by dilution and mixed layer depth in the Western Weddell-Scotia Confluence (WSC). *Mar. Ecol. Prog. Ser.* 366, 15–29.

Hofmann, E.E., Klinck, J.M., Lascara, C.M., Smith, D.A., 1996. Water mass distribution and circulation west of the Antarctic Peninsula and including Bransfield Strait. In: Ross, R.M., Hofmann, E.E., Quetin, L.B. (Eds.), *Foundations for Ecological Research West of the Antarctic Peninsula*, AGU Antarctic Research Series, vol. 70; 1996, pp. 61–80.

Holm-Hansen, O., Hewes, C.D., Villafane, V.E., Helbling, E.W., Silva, N., Amos, T., 1997. Distribution of phytoplankton and nutrients in relation to different water masses in the area around Elephant Island, Antarctica. *Polar Biol.* 18, 145–153.

Holm-Hansen, O., Kahru, M., Hewes, C.D., Kawaguchi, S., Kameda, T., Sushin, V., Krasovski, I., Priddle, J., Korb, R., Hewitt, R.P., Mitchell, B.G., 2004. Temporal and spatial distribution of chlorophyll-a in surface waters of the Scotia Sea as

- determined by both shipboard measurements and satellite data. *Deep-Sea Res. II* 51, 1323–1331.
- Hopkinson, B.M., Mitchell, G.B., Reynolds, R.A., Wang, H., Measures, C.I., Selph, K.E., Hewes, C.D., Holm-Hansen, O., Barbeau, K.A., 2007. Iron limitation across chlorophyll gradients in the southern Drake Passage: phytoplankton responses to iron addition and photosynthetic indicators of iron stress. *Limnol. Oceanogr.* 52, 2540–2554.
- Hoppema, M., Goeyens, L., 1999. Redfield behavior of carbon, nitrogen and phosphorus depletions in Antarctic surface water. *Limnol. Oceanogr.* 44, 220–224.
- Kahru, M., Mitchell, B.G., Gille, S.T., Hewes, C.D., Holm-Hansen, O., 2007. Eddies enhance biological production in the Weddell-Scotia Confluence of the Southern Ocean. *Geophys. Res. Lett.* 34, 114603, <http://dx.doi.org/10.1029/2007GL030430>.
- Karstensen, J., Tomczak, M., 1998. Age determination of mixed water masses using CFC and oxygen data. *J. Geophys. Res.* 103, 18599–18609.
- Karstensen, J., Tomczak, M., 2005. OMP Analysis Package for Matlab Version 2.0. <http://www.ldeo.columbia.edu/jkarsten/omp_std/README.html>, Lamont-Doherty Earth Observatory.
- Lipsky, J.D., 2004. AMLR 2003/2004 Field Season Report: Objectives, Accomplishments and Tentative Conclusions. Technical Report. NOAA-TM-NMFS-SWFSC-367. National Oceanic and Atmospheric Administration, December.
- Martin, J., Gordon, R., Fitzwater, S., 1990. Iron in Antarctic waters. *Nature* 345, 156–158.
- Measures, C.I., Landing, W.M., Brown, M.T., Buck, C.S., 2008. A commercially available rosette system for trace metal clean sampling. *Limnol. Oceanogr. Methods* 6, 384–394.
- Measures, C.I., Brown, M.T., Selph, K.E., April, A., Zhou, M., Hatta, M., Hiscock, W.T., 2013. The influence of shelf processes in delivering dissolved iron to the HNLC waters of the Drake Passage, Antarctica. *Deep-Sea Res. II* 90, 77–88.
- Niiler, P.P., Amos, A., Hu, J., 1991. Water masses and 200 m relative geostrophic circulation in the western Bransfield Strait region. *Deep-Sea Res. I* 38, 943–959.
- Orsi, A.H., Whitworth, T., Nowlin, W.D., 1995. On the meridional extent and fronts of the Antarctic Circumpolar Current. *Deep-Sea Res. I* 42, 641–673.
- Press, W.H., Flanner, B.P., Teukolsky, S.A., Vetterling, W.T., 1986. *Numerical Recipes: The Art of Scientific Computing*. Bridge University Press, pp. 502–504 (Chapter 14).
- Redfield, A.C., Ketchum, B.H., Richards, F.A., 1963. *The Influence of Organisms on the Composition of Sea-Water*, vol. 2. John Wiley and Sons Ltd. pp. 26–77.
- Silva, S.N., Helbling, E.W., Villafane, V.E., Amos, A.F., Holm-Hansen, O., 1995. Variability in nutrient concentrations around Elephant Island Antarctica, during 1991–1993. *Polar Res.* 14, 69–82.
- Sokolov, S., Rintoul, S.R., 2007. On the relationship between fronts of the Antarctic Circumpolar Current and surface chlorophyll concentrations in the Southern Ocean. *J. Geophys. Res.* 112, c07030, <http://dx.doi.org/10.1029/2006JC004072>.
- Sullivan, C.W., Arrigo, K.R., McClain, C.R., Comiso, J.C., Firestone, J., 1993. Distribution of phytoplankton blooms in the Southern Ocean. *Science* 262, 1832–1837.
- Takeda, S., 1998. Influence of iron availability on nutrient consumption ratios of diatoms in oceanic waters. *Nature* 393, 774–777.
- Thompson, A.F., Gille, S.T., MacKinnon, J.A., Sprintall, J., 2007. Spatial and temporal patterns of small-scale mixing in Drake Passage. *J. Phys. Oceanogr.* 37, 572–592.
- Thompson, A.F., Heywood, K.J., Thorpe, S.E., Renner, A.H.H., Travinca, A., 2009. Surface circulation at the tip of the Antarctic Peninsula from drifters. *J. Phys. Oceanogr.* 39 <http://dx.doi.org/10.1175/2008JPO3995.1171>.
- Timmermans, K.R., van der Wagt, B., de Baar, H.J.W., 2004. Growth rates, half-saturation constants, and silicate, nitrate and phosphate depletion in relation to iron availability of four large, open-ocean diatoms from the Southern Ocean. *Limnol. Oceanogr.* 49, 2141–2151.
- Tomczak, M., 1981. A multiparameter extension of temperature/salinity diagram techniques for the analysis of non-isopycnal mixing. *Prog. Oceanogr.* 10, 147–171.
- Tomczak, M., Large, D.G.B., 1989. Optimum multiparameter analysis of mixing in the thermocline of the Eastern Indian Ocean. *J. Geophys. Res.* 94, 16141–16149.
- Tomczak, M., Liefink, S., 2005. Interannual variations of water mass volumes in the Southern Ocean. *J. Atmos. Ocean Sci.* 10, 31–42.
- Tomczak, M., Poole, R., 1999. Optimum multiparameter analysis of the water mass structure in the Atlantic Ocean thermocline. *Deep-Sea Res. I* 46, 1895–1921.
- Venables, H.J., Pollard, R.T., Popova, E.E., 2007. Physical conditions controlling the development of a regular phytoplankton bloom north of the Crozet Plateau, Southern Ocean. *Deep-Sea Res. II* 54, 1949–1965.
- von Gyldenfeldt, A.-B., Fahrbach, E., Garcia, M.A., Schroder, M., 2002. Flow variability at the tip of the Antarctic Peninsula. *Deep-Sea Res. II* 49, 4743–4766.
- Whitehouse, M.J., Korb, R.E., Atkinson, A., Thorpe, S.E., Gordon, M., 2008. Formation, transport and decay of an intense phytoplankton bloom within the High-Nutrient Low-Chlorophyll belt of the Southern Ocean. *J. Mar. Syst.* 70, 150–167.
- Whitworth, T., Nowlin, W.D., Orsi, A.H., Locarnini, R.A., Smith, S.G., 1994. Weddell Sea shelf water in the Bransfield Strait and Weddell-Scotia Confluence. *Deep-Sea Res. I* 41, 629–641.
- You, Y., Tomczak, M., 1993. Thermocline circulation and ventilation in the Indian Ocean derived from water mass analysis. *Deep Sea Res.* 40, 13–56.
- Zhou, M., Niiler, P.P., Hu, J., 2002. Surface currents in the Bransfield and Gerlache Straits, Antarctica. *Deep-Sea Res. I* 49, 267–280.
- Zhou, M., Niiler, P.P., Zhu, Y., Dorland, R.D., 2006. The western boundary current in the Bransfield Strait, Antarctica. *Deep-Sea Res. I* 53, 1244–1252.
- Zhou, M., Zhu, Y., Dorland, R., 2010a. Dynamics of the current system in the Southern Drake Passage. *Deep-Sea Res.* 57, 1039–1048.
- Zhou, M., Zhu, Y., Dorland, R.D., Measures, C.I., 2010b. Dynamics of the current system in the southern Drake Passage. *Deep-Sea Res. I* 57, 1039–1048.